Nonrelativistic double photoeffect on *K*-shell electrons

A. I. Mikhailov,[1,2] I. A. Mikhailov,[1] A. N. Moskalev,[1] A. V. Nefiodov,[1,2] G. Plunien,[2] and G. Soff[2]
[1]*Petersburg Nuclear Physics Institute, 188300 Gatchina, St. Petersburg, Russia*
[2]*Institut für Theoretische Physik, Technische Universität Dresden, Mommsenstraße 13, D-01062 Dresden, Germany*
(Received 15 August 2003; revised manuscript received 7 November 2003; published 9 March 2004)

We investigate the double *K*-shell ionization of heliumlike ions caused by the absorption of a single photon with energies being much smaller than the rest energy of an electron. In the near-threshold region, differential and total cross sections of the process are calculated for light ions, taking into account the leading orders of the $1/Z$ and αZ expansions. QED perturbation theory with respect to the parameter $1/Z$ exhibits a fast convergence in the entire nonrelativistic domain for moderate nuclear charge numbers $Z \geqslant 2$. Going beyond the electric dipole approximation leads to a forward/backward asymmetry in the angular distributions for the ejected electrons with respect to the incident photon beam. A comparison of theoretical predictions for the ratio of double-to-single photoionization cross sections with available experimental data for a number of neutral atoms is also presented.

DOI: 10.1103/PhysRevA.69.032703 PACS number(s): 32.80.Fb, 31.25.−v, 32.30.Rj, 33.60.Fy

I. INTRODUCTION

In studies of electron correlations in atoms, the most attractive processes are those in which the electron-electron interaction plays the crucial role. One of such fundamental phenomena is the double photoionization of an atom caused by the absorption of a single photon, the so-called double photoeffect, which has been investigated for more than 30 years [1–3]. Since a photon interacts only with a single electron, the simultaneous ejection of two electrons is exclusively caused by the electron-electron interaction. Accordingly, electron correlations show up here most clearly.

So far the experiments have been mainly performed with helium, the simplest many-electron atomic system. The majority of investigations concerns the energy dependence of the ratio R of double-to-single photoionization cross sections [4–6]. With increasing photon energy ω, the ratio R grows rapidly beyond the ionization threshold. Then, after having a maximum near the threshold, it declines slowly approaching the constant limit of 1.72(12)% [7] in the asymptotic domain of nonrelativistic photon energies being much larger than the threshold energy I_{2K} for double ionization from the K shell, that is, $I_{2K} \ll \omega \ll m$, where m is the electron mass ($\hbar = c = 1$). Although a fair agreement between theory and experimental data has been achieved within a wide range of photon energies [8], one of the most frequent problems in theoretical descriptions of the double photoionization is the gauge dependence of numerical results [9].

Atomic targets with nuclear charge number $Z \geqslant 3$ have been investigated much less thoroughly. In Ref. [10], cross sections σ^{++} for double K-shell photoionization were measured for a few elements within the range $22 \leqslant Z \leqslant 28$ and for photon energies somewhat above the threshold. Recent developments of novel synchrotron radiation sources allow one to perform experiments with intense collimated beams of tunable monochromatic x rays in the keV regime. Measurements of the ratio R of double-to-single K-vacancy production by photon impact have been reported for Mo [11], Cu [12], and Ne [13] at various photon energies as well as for Ca, Ti, and V in the energy range of 8–35 keV [14]. This represents a challenge to theoretical investigations of the process in the entire nonrelativistic domain, both for photon energies $\omega \ll m$ and for targets with moderate values of nuclear charge numbers Z. In Refs. [15–17], a Z-scaling law was suggested for the ratio R of double-to-single photoionization cross sections in the asymptotic energy regime, $I_{2K} \ll \omega \ll m$. For the energy domain near the threshold, $\omega \simeq I_{2K}$, *ab initio* calculations are presently not available. To compare with the experiment, one usually employs a model estimate of the two-electron photoejection cross section σ^{++} obtained by Kornberg and Miraglia [18], which however strongly disagrees with existing experimental data. Numerical calculations of $Z^4\sigma^{++}$ for He, Li^+, and O^{6+} have been also performed within the framework of the convergent close-coupling model [19].

Another direction of present investigations concerns the angular distributions of atomic photoelectrons beyond the dipole approximation. However, until now these studies have been limited to single photoionization only [20–29]. Beyond the dipole approximation, the reflection symmetry of angular distributions with respect to the plane perpendicular to the light beam is violated [30]. We shall show that there exists a rather wide domain of nonrelativistic photon energies, where nondipole effects become also important in the case of double K-shell ionization. The cross sections of the process turn out to be rather sensitive to the explicit electron-photon interaction.

In the present paper, we employ the perturbation theory with respect to the electron-electron interaction. As a zeroth approximation, Coulomb wave functions and Coulomb Green's functions are utilized. The study is performed for photon energies much smaller than the electron rest energy. Accordingly, all electrons involved in the ionization process are considered as being nonrelativistic. This implies the smallness of the Coulomb parameter, that is, $\alpha Z \ll 1$, where $\alpha = e^2$ is the fine-structure constant. However, the nuclear charge number Z is supposed to be high enough to utilize $1/Z$ as expansion parameter. The accuracy of our results is restricted by higher-order terms of order $1/Z^2$ and $(\alpha Z)^2$, which are omitted in the present investigation. A similar ap-

proach has been already used in the asymptotic part of the nonrelativistic domain, $I_{2K} \ll \omega \ll m$, where all formulas can be significantly simplified [15]. In contrast to Ref. [15], we consider the entire nonrelativistic domain of incident photon energies with special emphasis on the threshold region. The results obtained are applicable for heliumlike ions with $2 \leqslant Z \leqslant 35$ and $I_{2K} \leqslant \omega \leqslant 150$ keV. Since *K*-shell electrons are essentially separated from the other electrons in an atom, it turns out that our formulas also describe fairly well the double *K*-shell ionization in the case of light neutral atoms.

II. THE AMPLITUDE OF DOUBLE PHOTOIONIZATION IN THE DIPOLE DOMAIN OF PHOTON ENERGIES

The domain of photon energies near the threshold of double photoionization corresponds to the dipole regime characterized by $\omega \ll \eta$, where $\eta = m\alpha Z$ is the average momentum of a *K*-shell electron. Neglecting terms of the order of $(\alpha Z)^2$, the operator describing the interaction between a photon and an electron reads [31]

$$\hat{\gamma} = -\frac{e}{m}\frac{\sqrt{4\pi}}{\sqrt{2\omega}}\left\{(\mathbf{e}\cdot\hat{\boldsymbol{p}}) + \frac{i}{2}(\mathbf{e}\cdot[\boldsymbol{\sigma},\boldsymbol{k}])\right\} e^{i(\boldsymbol{k}\cdot\boldsymbol{r})}, \tag{1}$$

where $\hat{\boldsymbol{p}}$ is the momentum operator of an electron, $\boldsymbol{\sigma}$ is the vector of the Pauli matrices, $\boldsymbol{k}$ is the photon wave vector, and $\omega = |\boldsymbol{k}| = k$ and $\mathbf{e}$ are the energy and the polarization vector of a photon, respectively. We employ here the Coulomb gauge, in which $(\mathbf{e}\cdot\boldsymbol{k}) = 0$ and $(\mathbf{e}^*\cdot\mathbf{e}) = 1$. The first term in Eq. (1) describes the orbital part of the interaction, while the second term accounts for the spin-dependent contribution. As the result of acting with $\hat{\gamma}$ on electronic wave functions, the operator $\hat{\boldsymbol{p}}$ substitutes by the characteristic momenta of the problem. Near the threshold, the latter are values of the same order of η. It also implies that the process occurs at atomic distances of the order of the *K*-shell radius. Therefore, the second term in Eq. (1) can be neglected.

In the nonrelativistic approximation, spatial and spin parts of two-electron wave functions are factorized. For the *K* shell, the spin function is antisymmetric (singlet), while the spatial function is symmetric. Since in the dipole domain of photon energies the electron-photon interaction does not depend on the electron spin, the symmetry of the spin function is not changed in the ionization process. As a result, the spin function can be suppressed throughout the consideration. While the total wave function transforms antisymmetrically under the interchange of electrons, its spatial part $\Psi(\boldsymbol{r}_1,\boldsymbol{r}_2)$ remains symmetrical. Consequently, it is sufficient to consider the interaction of an incoming photon with a single atomic electron only. The total amplitude of the process takes the form

$$\mathcal{A} = 2\langle\Psi_f|\hat{\gamma}|\Psi_i\rangle, \tag{2}$$

where the factor 2 takes into account that both electrons interact with a photon [compare with Eq. (70)].

The wave functions $\Psi_{i,f}$ may be derived in first-order perturbation theory with respect to the electron-electron interaction, i.e., $\Psi_{i,f} \simeq \Psi_{i,f}^{(0)} + \Psi_{i,f}^{(1)}$. Accordingly, due to the one-particle character of the operator $\hat{\gamma}$, one obtains

$$\mathcal{A} = 2\langle\Psi_f^{(0)}|\hat{\gamma}|\Psi_i^{(1)}\rangle + 2\langle\Psi_f^{(1)}|\hat{\gamma}|\Psi_i^{(0)}\rangle. \tag{3}$$

As a zeroth approximation, we shall utilize the single-particle approximation in the Coulomb field of the nucleus (Furry picture):

$$\Psi_i^{(0)}(\boldsymbol{r}_1,\boldsymbol{r}_2) = \psi_{1s}(\boldsymbol{r}_1)\psi_{1s}(\boldsymbol{r}_2), \tag{4}$$

$$\Psi_f^{(0)}(\boldsymbol{r}_1,\boldsymbol{r}_2) = \frac{1}{\sqrt{2}}[\psi_{\boldsymbol{p}_1}(\boldsymbol{r}_1)\psi_{\boldsymbol{p}_2}(\boldsymbol{r}_2) + \psi_{\boldsymbol{p}_1}(\boldsymbol{r}_2)\psi_{\boldsymbol{p}_2}(\boldsymbol{r}_1)]. \tag{5}$$

Here $\boldsymbol{p}_1$ and $\boldsymbol{p}_2$ are the momenta of escaping electrons at infinity. The first-order corrections to the wave functions are found from the following equations [32]:

$$\Psi_i^{(1)}(\boldsymbol{r}_1,\boldsymbol{r}_2) = (E_i^{(0)} - H_1 - H_2)^{-1}(1-\mathcal{P}_i)V_{12}\Psi_i^{(0)}(\boldsymbol{r}_1,\boldsymbol{r}_2), \tag{6}$$

$$\Psi_f^{(1)}(\boldsymbol{r}_1,\boldsymbol{r}_2) = (E_f^{(0)} - H_1 - H_2 + i\epsilon)^{-1}V_{12}\Psi_f^{(0)}(\boldsymbol{r}_1,\boldsymbol{r}_2). \tag{7}$$

Here $E_i^{(0)} = 2E_{1s}$ with E_{1s} being the single-electron energies in the initial bound state $\Psi_i^{(0)}$, $\mathcal{P}_i = |\Psi_i^{(0)}\rangle\langle\Psi_i^{(0)}|$ is the projection operator on this state, $E_f^{(0)} = E_{p_1} + E_{p_2}$, where E_{p_1} and E_{p_2} are the electron energies in the final continuum state $\Psi_f^{(0)}$, and H_1 and H_2 are the single-particle Hamiltonians for an electron in the Coulomb field of the nucleus. In Eq. (7), the infinitesimal number ϵ is assumed to be positive. In the coordinate representation, the operator V_{12} of the electron-electron Coulomb interaction is given by $V_{12} = \alpha/r_{12}$, where $r_{12} = |\boldsymbol{r}_1 - \boldsymbol{r}_2|$.

Inserting Eqs. (4)–(7) into Eq. (3), the amplitude $\mathcal{A}$ describing the double photoeffect of the atomic *K* shell is represented by the sum of four terms,

$$\mathcal{A} = \sqrt{2}[\mathcal{A}_a + \mathcal{A}_b + \mathcal{A}_c + \mathcal{A}_d], \tag{8}$$

where

$$\mathcal{A}_a = \langle\psi_{\boldsymbol{p}_1}\psi_{\boldsymbol{p}_2}|\hat{\gamma}G_C(E_a)V_{12}|\psi_{1s}\psi_{1s}\rangle, \tag{9}$$

$$\mathcal{A}_b = \langle\psi_{\boldsymbol{p}_1}\psi_{\boldsymbol{p}_2}|V_{12}G_C(E_b)\hat{\gamma}|\psi_{1s}\psi_{1s}\rangle, \tag{10}$$

$$\mathcal{A}_c = \langle\psi_{\boldsymbol{p}_2}\psi_{\boldsymbol{p}_1}|\hat{\gamma}G_C(E_c)V_{12}|\psi_{1s}\psi_{1s}\rangle, \tag{11}$$

$$\mathcal{A}_d = \langle\psi_{\boldsymbol{p}_2}\psi_{\boldsymbol{p}_1}|V_{12}G_C(E_b)\hat{\gamma}|\psi_{1s}\psi_{1s}\rangle. \tag{12}$$

Here $G_C(E) = (E - H_1)^{-1}$ denotes the single-particle Coulomb Green's function with the energy *E*. In Eqs. (9)–(12), the intermediate energies are defined as follows:

$$E_a = 2E_{1s} - E_{p_2}, \tag{13}$$

$$E_c = 2E_{1s} - E_{p_1}, \tag{14}$$

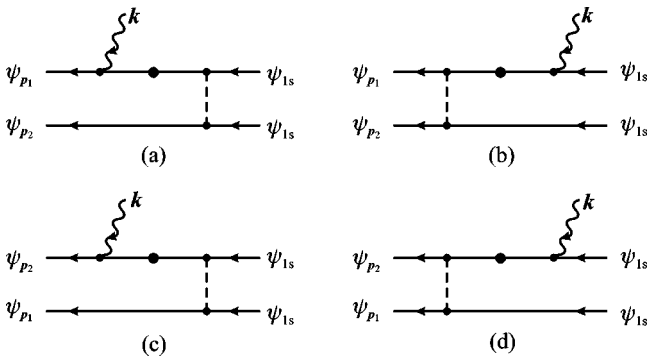

FIG. 1. Feynman diagrams for the double ionization of the atomic *K* shell by a single photon. Solid lines denote electrons in the Coulomb field of the nucleus, the dashed line denotes the electron-electron Coulomb interaction, and the wavy line denotes an incident photon. The line with a heavy dot corresponds to the Coulomb Green function. For this line, only the energy is conserved, while the momentum is violated due to the interaction with a nucleus. Diagrams (a) and (c) take into account the electron-electron interaction in the initial state, while diagrams (b) and (d) account for it in the final state.

$$E_b = E_{p_1} + E_{p_2} - E_{1s} = \omega + E_{1s}. \tag{15}$$

The latter relation results here from the energy-conservation law, $E_f^{(0)} = \omega + E_i^{(0)}$. We assume also that $I_{2K} = 2I$, where $I = \eta^2/(2m)$ is the Coulomb potential for single ionization. In the double photoionization, a photon energy is distributed between two electrons. As a result, an outgoing electron can have any energy in the range between 0 and $\omega - I_{2K}$. In the following we shall assume that $p_1 \geqslant p_2$. Accordingly, the electron labeled by the index 1 is referred to as the fast one, while the second electron is referred to as the slow one.

The matrix elements given by Eqs. (9)–(12) can be represented by the Feynman graphs depicted in Fig. 1. In any vertex the energy-momentum conservation is supposed to be valid. The integrations are performed over all intermediate momenta. In the momentum representation, the photon vertex corresponds to the following operator:

$$\langle \boldsymbol{f}' | \hat{\gamma} | \boldsymbol{f} \rangle = \frac{1}{m} \frac{\sqrt{4\pi\alpha}}{\sqrt{2\omega}} (\mathbf{e} \cdot \boldsymbol{f}) \langle \boldsymbol{f}' | \boldsymbol{f} + \boldsymbol{k} \rangle. \tag{16}$$

Here the plane-wave states are normalized to δ function in the momenta,

$$\langle \boldsymbol{f}' | \boldsymbol{f} \rangle = (2\pi)^3 \delta(\boldsymbol{f}' - \boldsymbol{f}). \tag{17}$$

The electron-electron interaction V_{12} corresponds to the photon propagator $D(\boldsymbol{f}) = 4\pi\alpha/\boldsymbol{f}^2$, which describes an exchange of the Coulomb photon.

Let us derive first the expression for the amplitude $\mathcal{A}_a$. It can be written as follows:

$$\mathcal{A}_a = \frac{1}{m} \frac{\sqrt{4\pi\alpha}}{\sqrt{2\omega}} \int \frac{d\boldsymbol{f}}{(2\pi)^3} F_a(\boldsymbol{p}_1, \boldsymbol{f}) D(\boldsymbol{f}) F(\boldsymbol{p}_2, \boldsymbol{f}), \tag{18}$$

$$F_a(\boldsymbol{p}_1, \boldsymbol{f}) = \int \frac{d\boldsymbol{f}'}{(2\pi)^3} \frac{d\boldsymbol{f}_1}{(2\pi)^3} \langle \psi_{\boldsymbol{p}_1} | \boldsymbol{f}' + \boldsymbol{k} \rangle (\mathbf{e} \cdot \boldsymbol{f}') \times \langle \boldsymbol{f}' | G_C(p_a) | \boldsymbol{f}_1 \rangle \langle \boldsymbol{f}_1 + \boldsymbol{f} | \psi_{1s} \rangle, \tag{19}$$

$$F(\boldsymbol{p}_2, \boldsymbol{f}) = \int \frac{d\boldsymbol{f}_2}{(2\pi)^3} \langle \psi_{\boldsymbol{p}_2} | \boldsymbol{f}_2 \rangle \langle \boldsymbol{f}_2 - \boldsymbol{f} | \psi_{1s} \rangle. \tag{20}$$

In Eq. (19), $p_a = \sqrt{2mE_a + i0}$ is the momentum of an electron in the intermediate state for the diagram in Fig. 1(a). In the momentum representation, the wave function of the $1s$ state can be expressed as follows:

$$\langle \boldsymbol{f}' - \boldsymbol{f} | \psi_{1s} \rangle = N_{1s} \left(-\frac{\partial}{\partial \eta} \right) \langle \boldsymbol{f}' | V_{i\eta} | \boldsymbol{f} \rangle, \tag{21}$$

$$\langle \boldsymbol{f}' | V_{i\eta} | \boldsymbol{f} \rangle = \frac{4\pi}{(\boldsymbol{f}' - \boldsymbol{f})^2 + \eta^2}. \tag{22}$$

Here the normalization factor N_{1s} is defined by $N_{1s}^2 = \eta^3/\pi$ and $\eta = m\alpha Z$. Inserting the expression (21) into Eq. (20), one finally obtains

$$F(\boldsymbol{p}_2, \boldsymbol{f}) = N_{1s} \left(-\frac{\partial}{\partial \lambda} \right) \langle \psi_{\boldsymbol{p}_2} | V_{i\lambda} | \boldsymbol{f} \rangle_{|\lambda = \eta} \tag{23}$$

after the closure relation for the complete system of plane waves

$$\int \frac{d\boldsymbol{f}}{(2\pi)^3} |\boldsymbol{f}\rangle\langle\boldsymbol{f}| = 1 \tag{24}$$

has been used.

The Coulomb continuum wave functions can be represented as follows [30]:

$$\langle \psi_{\boldsymbol{p}} | \boldsymbol{f} \rangle = \frac{1}{2\pi i} N_p \left(-\frac{\partial}{\partial \varepsilon} \right) \oint^{(0^+, 1^+)} \frac{dt}{t} \left(\frac{-t}{1-t} \right)^{i\xi} \times \langle \boldsymbol{p}(1-t) | V_{pt + i\varepsilon} | \boldsymbol{f} \rangle_{|\varepsilon \to 0}, \tag{25}$$

$$N_p^2 = \frac{2\pi\xi}{1 - \exp(-2\pi\xi)},$$

where $\xi = \eta/p$. The integration contour in Eq. (25) is a closed curve enclosing counter-clockwise the points 0 and 1. After taking the derivative, the parameter ε should tend to zero. To calculate $F_a(\boldsymbol{p}_1, \boldsymbol{f})$, we make use of the identity

$$\langle \psi_{\boldsymbol{p}_1} | \boldsymbol{f}' + \boldsymbol{k} \rangle (\mathbf{e} \cdot \boldsymbol{f}') = N_{p_1} \hat{\mathcal{I}}_{\xi_1}(t) (\mathbf{e} \cdot \boldsymbol{\Gamma}) \langle \boldsymbol{\kappa} | V_{p_1 t + i\varepsilon} | \boldsymbol{f}' \rangle, \tag{26}$$

where $\boldsymbol{\kappa} = \boldsymbol{v}_1 - \boldsymbol{k}$, $\boldsymbol{v}_1 = \boldsymbol{p}_1(1-t)$, $\xi_1 = \eta/p_1$, $N_{p_1} = \exp(\pi\xi_1/2)|\Gamma(1 - i\xi_1)|$, and $\boldsymbol{\Gamma} = ip_1 t \boldsymbol{\nabla}_k - \boldsymbol{v}_1 \partial/\partial\varepsilon$ with $\boldsymbol{\nabla}_k$ being the gradient with respect to $\boldsymbol{k}$. In Eq. (26), we have introduced the integral operator

$$\hat{\mathcal{I}}_{\xi}(t)=\frac{1}{2\pi i}\oint^{(0^+,1^+)}\frac{dt}{t}\left(\frac{-t}{1-t}\right)^{i\xi}, \tag{27}$$

depending on the parameter ξ and acting on functions of the variable t.

With the aid of Eqs. (21) and (26), the expression (19) takes the following form:

$$F_a(\boldsymbol{p}_1,\boldsymbol{f})=N_{p_1}N_{1s}\hat{\mathcal{I}}_{\xi_1}(t)(\mathbf{e}\cdot\boldsymbol{\Gamma})\left(-\frac{\partial}{\partial\zeta}\right)\times\langle\boldsymbol{\kappa}|V_{i\nu}G_C(p_a)V_{i\xi}|-\boldsymbol{f}\rangle|_{\substack{\xi=\eta\\ \varepsilon\to 0}}, \tag{28}$$

where $i\nu=p_1t+i\varepsilon$. Using results of Refs. [33,34], the matrix element (28) can be transformed into the one-dimensional integral:

$$F_a(\boldsymbol{p}_1,\boldsymbol{f})=imN_{p_1}N_{1s}\hat{\mathcal{I}}_{\xi_1}(t)(\mathbf{e}\cdot\boldsymbol{\Gamma})\frac{\partial}{\partial\zeta}\times\int_0^1\frac{dx}{\Lambda_a}(\exp)_a\langle-\boldsymbol{\kappa}x|V_{\Lambda_a+i\zeta}|\boldsymbol{f}\rangle|_{\substack{\zeta=\eta\\ \varepsilon\to 0}}, \tag{29}$$

$$(\exp)_a=\exp\left\{i\eta\int_x^1\frac{dx'}{x'\Lambda_a'}\right\}=\left[\frac{1}{x}\frac{(\kappa x)^2-(p_a+\Lambda_a)^2}{\kappa^2-(p_a+i\nu)^2}\right]^{i\xi_a}, \tag{30}$$

$$\Lambda_a=\sqrt{(p_a^2-\kappa^2x)(1-x)-\nu^2x}, \tag{31}$$

where $p_a=\sqrt{2mE_a+i0}$ and $\xi_a=\eta/p_a$. In Eq. (30), Λ_a' is equal to Λ_a with the substitution of x by x'. Taking into account that the energy E_a of Green's function is defined according to Eq. (13), we obtain $i\xi_a=1/\sqrt{2+\varepsilon_2}$, where $\varepsilon_2=E_{p_2}/I$ and $I=\eta^2/(2m)$.

Inserting Eqs. (23) and (29) into Eq. (18) and taking into account the relation [30]

$$\int\frac{d\boldsymbol{f}}{(2\pi)^3}V_{i\lambda}|\boldsymbol{f}\rangle\frac{1}{\boldsymbol{f}^2}\langle\boldsymbol{f}|V_{\Lambda_a+i\zeta}|-\boldsymbol{\kappa}x\rangle=\frac{i}{2}\int_0^1\frac{dy}{\Omega_a}V_{\Omega_a+i\lambda}|-\boldsymbol{\kappa}xy\rangle, \tag{32}$$

where

$$\Omega_a=\sqrt{(\Lambda_a+i\zeta)^2y-(\kappa x)^2y(1-y)}, \tag{33}$$

we find the following expression for the amplitude:

$$\mathcal{A}_a=2\pi\alpha\frac{\sqrt{4\pi\alpha}}{\sqrt{2\omega}}N_{p_1}N_{1s}^2\hat{\mathcal{I}}_{\xi_1}(t)(\mathbf{e}\cdot\boldsymbol{\Gamma})\frac{\partial^2}{\partial\lambda\,\partial\zeta}\times\int_0^1dx\int_0^1dy\frac{(\exp)_a}{\Lambda_a\Omega_a}\langle\psi_{\boldsymbol{p}_2}|V_{\Omega_a+i\lambda}|-\boldsymbol{\kappa}xy\rangle. \tag{34}$$

The matrix element, which remains in the integrand of Eq. (34), can be calculated analytically [30]. Then one obtains the following compact representation for $\mathcal{A}_a$:

$$\mathcal{A}_a=8\pi^2\alpha\frac{\sqrt{4\pi\alpha}}{\sqrt{2\omega}}\mathcal{N}\hat{\mathcal{I}}_{\xi_1}(t)\int_0^1dx\int_0^1dy(\mathbf{e}\cdot\boldsymbol{\Gamma})\times\frac{\partial^2}{\partial\lambda\,\partial\zeta}\frac{(\exp)_a}{\Lambda_a\Omega_a}\frac{1}{W_a}\left(\frac{W_a}{Q_a}\right)\Bigg|^{i\xi_2}_{\substack{\lambda=\eta,\\ \zeta=\eta\\ \varepsilon\to 0}} \tag{35}$$

$$W_a=(\boldsymbol{\kappa}xy+\boldsymbol{p}_2)^2-(\Omega_a+i\lambda)^2, \tag{36}$$

$$Q_a=(\kappa xy)^2-(p_2+\Omega_a+i\lambda)^2, \tag{37}$$

where $\mathcal{N}=N_{p_1}N_{p_2}N_{1s}^2$ and $\xi_l=\eta/p_l$ $(l=1,2)$. After taking derivatives in Eq. (35), one should set $\zeta=\lambda=\eta$ and take the limit $\varepsilon\to 0$.

The amplitude $\mathcal{A}_b$ takes into account the electron-electron interaction in the final state, i.e., the Coulomb interaction between the electrons in the continuous spectrum. Usually, this final-state interaction is either not considered at all or treated effectively within the framework of some model-wave functions [18,35]. In the first approach, the so-called independent-electron approximation, one takes the product of two Coulomb continuum functions as the two-electron wave function. In the second case, the wave function is constructed as a product of even three Coulomb functions of the continuous spectrum. In the asymptotic nonrelativistic regime ($\omega\sim\eta$), the contribution of the graph in Fig. 1(b) to the total amplitude of the process turns out to be of minor importance and therefore it might be neglected. However, in the dipole domain of photon energies ($\omega\ll\eta$), one should take into account all the graphs together.

Let us represent the amplitude $\mathcal{A}_b$ in the form analogous to Eq. (18),

$$\mathcal{A}_b=\frac{1}{m}\frac{\sqrt{4\pi\alpha}}{\sqrt{2\omega}}\int\frac{d\boldsymbol{f}}{(2\pi)^3}F_b(\boldsymbol{p}_1,\boldsymbol{f})D(\boldsymbol{f})F(\boldsymbol{p}_2,\boldsymbol{f}), \tag{38}$$

$$F_b(\boldsymbol{p}_1,\boldsymbol{f})=\int\frac{d\boldsymbol{f}'}{(2\pi)^3}\frac{d\boldsymbol{f}_1}{(2\pi)^3}\langle\psi_{\boldsymbol{p}_1}|\boldsymbol{f}'-\boldsymbol{f}\rangle\langle\boldsymbol{f}'|G_C(p_b)|\boldsymbol{f}_1\rangle\times(\mathbf{e}\cdot\boldsymbol{f}_1)\langle\boldsymbol{f}_1-\boldsymbol{k}|\psi_{1s}\rangle. \tag{39}$$

The matrix element $F(\boldsymbol{p}_2,\boldsymbol{f})$ is defined by formulas (20) and (23). Performing similar steps as for the calculation of $\mathcal{A}_a$, we derive

$$\int\frac{d\boldsymbol{f}_1}{(2\pi)^3}\langle\boldsymbol{f}'|G_C(p_b)|\boldsymbol{f}_1\rangle(\mathbf{e}\cdot\boldsymbol{f}_1)\langle\boldsymbol{f}_1-\boldsymbol{k}|\psi_{1s}\rangle=N_{1s}\eta(\mathbf{e}\cdot\boldsymbol{\nabla}_k)\langle\boldsymbol{f}|G_C(p_b)V_{i\eta}|\boldsymbol{k}\rangle. \tag{40}$$

Accordingly, Eq. (39) can be cast into the following form:

$$F_b(\boldsymbol{p}_1,\boldsymbol{f})=\eta N_{p_1}N_{1s}\hat{\mathcal{I}}_{\xi_1}(t)\left(-\frac{\partial}{\partial\varepsilon}\right)(\mathbf{e}\cdot\boldsymbol{\nabla}_k)\times\langle\boldsymbol{v}_1+\boldsymbol{f}|V_{i\nu}G_C(p_b)V_{i\eta}|\boldsymbol{k}\rangle, \tag{41}$$

where $\boldsymbol{v}_1$ and ν are the same as in Eqs. (26) and (28). Inserting the expressions (23) and (41) into Eq. (38) and performing the integration over $\boldsymbol{f}$, we find

$$\mathcal{A}_b = 8\pi^2\alpha\frac{\sqrt{4\pi\alpha}}{\sqrt{2\omega}}\mathcal{N}\eta\hat{\mathcal{I}}_{\xi_1}(t)\int_0^1 dx\int_0^1 dy(\mathbf{e}\cdot\boldsymbol{\nabla}_k)\times\frac{\partial^2}{\partial\varepsilon\partial\lambda}\frac{(\exp)_b}{\Lambda_b\Omega_b}\frac{1}{W_b}\left(\frac{W_b}{Q_b}\right)\Bigg|_{\substack{\lambda=\eta\\ \varepsilon\to 0}}^{i\xi_2}, \tag{42}$$

$$(\exp)_b = \left[\frac{1}{x}\frac{(p_b+\Lambda_b)^2-(kx)^2}{(p_b+i\eta)^2-k^2}\right]^{i\xi_b}, \tag{43}$$

$$\Lambda_b = \sqrt{(p_b^2-k^2x)(1-x)-\eta^2x}, \tag{44}$$

$$\Omega_b = \sqrt{(\Lambda_b+p_1t+i\varepsilon)^2y-q^2y(1-y)}, \tag{45}$$

$$W_b = (\boldsymbol{q}y+\boldsymbol{p}_2)^2-(\Omega_b+i\lambda)^2, \tag{46}$$

$$Q_b = (qy)^2-(p_2+\Omega_b+i\lambda)^2. \tag{47}$$

Here $\boldsymbol{q}=\boldsymbol{v}_1-\boldsymbol{k}x$, $\xi_b=\eta/p_b$, and $p_b=\sqrt{2mE_b}$ with $E_b=\omega-I$ being the electron energy in the intermediate state of the diagram in Fig. 1(b). The momentum of the electron p_b should be understood as $\sqrt{p_b^2+i0}$ [33]. This choice fixes the branch of the multivalued function Λ_b with respect to the variable x.

The amplitudes $\mathcal{A}_c$ and $\mathcal{A}_d$ corresponding to the exchange graphs in Figs. 1(c) and 1(d), respectively, can be derived from Eqs. (35) and (42) by interchanging $p_1\rightleftharpoons p_2$. However, the resulting expressions appear to be inconvenient for further numerical calculations. The contour integral over the variable t depends now on the value ξ_2, which can reach very large values when $p_2\to 0$. Since we have chosen $p_1\geqslant p_2$ and due to the energy-conservation law $E_{p_1}+E_{p_2}=\omega-I_{2K}$, one is faced with the limiting case $p_2\to 0$ or, equivalently, $\xi_2\to\infty$. Thus the integrand is a strongly oscillating function for any $\omega>I_{2K}$. Therefore, it is better to rederive the expressions for $\mathcal{A}_c$ and $\mathcal{A}_d$ in a more convenient form. From the two contour integrals representing the continuum wave functions, only that integral is evaluated analytically which depends on the parameter ξ_2. The final expressions for $\mathcal{A}_c$ and $\mathcal{A}_d$ will look similar to Eqs. (35) and (42).

For numerical integration, it is convenient to transform the contour integral into an ordinary one according to the following relation [36]:

$$\hat{\mathcal{I}}_\xi(t)f(t) = f(0)-\frac{\sinh(\pi\xi)}{\pi i}\int_0^1\frac{dt}{t}\left(\frac{t}{1-t}\right)^{i\xi}[f(t)-f(0)]. \tag{48}$$

The formulas (35) and (42) are still inconvenient for direct numerical computations because of the presence of the operator $(\mathbf{e}\cdot\boldsymbol{\nabla}_k)$. Although the expressions become somewhat more complicated, the vector differentiation should be performed analytically. With the aid of Eq. (48), we obtain

$$\mathcal{A}_a = (4\pi)^2\alpha\frac{\sqrt{4\pi\alpha}}{\sqrt{2\omega}}\mathcal{M}[(\mathbf{e}\cdot\boldsymbol{n}_1)F_1+(\mathbf{e}\cdot\boldsymbol{n}_2)F_2], \tag{49}$$

$$F_l = f_l(0)-\frac{\sinh(\pi\xi_1)}{\pi i}\int_0^1\frac{dt}{t}\left(\frac{t}{1-t}\right)^{i\xi_1}[f_l(t)-f_l(0)] \quad (l=1,2), \tag{50}$$

$$f_1(t) = -v_1\int_0^1 dx\int_0^1 dy\frac{\partial^2}{\partial\lambda\partial\zeta}\times\left(ip_1t\frac{\partial'}{\partial\kappa^2}+\frac{1}{2}\frac{\partial}{\partial\varepsilon}\right)\frac{(\exp)_a}{\Lambda_a\Omega_a}\frac{1}{W_a}\left(\frac{W_a}{Q_a}\right)^{i\xi_2}, \tag{51}$$

$$f_2(t) = (\eta+ip_2)p_1t\int_0^1 dx\int_0^1 dy\frac{\partial^2}{\partial\lambda\partial\zeta}\frac{(\exp)_a}{\Lambda_a\Omega_a}\frac{xy}{W_a^2}\left(\frac{W_a}{Q_a}\right)^{i\xi_2}, \tag{52}$$

where $\boldsymbol{n}_l=\boldsymbol{p}_l/p_l$ $(l=1,2)$ are unit vectors of electron momenta. The prime at the derivative with respect to κ^2 in Eq. (51) implies that it does not act on the scalar product $(\boldsymbol{\kappa}\cdot\boldsymbol{p}_2)$, which appears in W_a.

Similar expressions can be obtained for other amplitudes. The contribution corresponding to the graph in Fig. 1(b) is given by

$$\mathcal{A}_b = (4\pi)^2\alpha\frac{\sqrt{4\pi\alpha}}{\sqrt{2\omega}}\mathcal{N}\eta[(\mathbf{e}\cdot\boldsymbol{n}_1)\Phi_1+(\mathbf{e}\cdot\boldsymbol{n}_2)\Phi_2], \tag{53}$$

$$\Phi_l = \varphi_l(0)-\frac{\sinh(\pi\xi_1)}{\pi i}\int_0^1\frac{dt}{t}\left(\frac{t}{1-t}\right)^{i\xi_1}[\varphi_l(t)-\varphi_l(0)] \quad (l=1,2), \tag{54}$$

$$\varphi_1(t) = -v_1\int_0^1 dx\int_0^1 dy\frac{\partial^2}{\partial\varepsilon\partial\lambda}\frac{\partial'}{\partial q^2}\frac{(\exp)_b}{\Lambda_b\Omega_b}\frac{x}{W_b}\left(\frac{W_b}{Q_b}\right)^{i\xi_2}, \tag{55}$$

$$\varphi_2(t) = -i(\eta+ip_2)\int_0^1 dx\int_0^1 dy\frac{\partial^2}{\partial\varepsilon\partial\lambda}\frac{(\exp)_b}{\Lambda_b\Omega_b}\frac{xy}{W_b^2}\left(\frac{W_b}{Q_b}\right)^{i\xi_2}. \tag{56}$$

Again $\partial'/\partial q^2$ in Eq. (55) indicates that it does not act on the product $(\boldsymbol{q}\cdot\boldsymbol{p}_2)$ in W_b.

The resulting expressions for the exchange amplitudes corresponding to the Feynman diagrams in Figs. 1(c) and 1(d) will be given explicitly without derivation. The contribution due to the graph in Fig. 1(c) reads

$$\mathcal{A}_c = (4\pi)^2\alpha\frac{\sqrt{4\pi\alpha}}{\sqrt{2\omega}}\mathcal{M}[(\mathbf{e}\cdot\boldsymbol{n}_1)\tilde{F}_1+(\mathbf{e}\cdot\boldsymbol{n}_2)\tilde{F}_2], \tag{57}$$

$$\tilde{f}_1(t) = -v_1\eta\int_0^1 dx\int_0^1 dy\frac{\partial^2}{\partial\lambda\partial\zeta}\frac{(\exp)_c}{\Lambda_c\Omega_c}\frac{xy}{W_cQ_c}\left(\frac{W_c}{Q_c}\right)^{i\xi_2}, \tag{58}$$

$$\tilde{f}_2(t)=-(\eta+ip_2)\int_0^1 dx\int_0^1 dy\,\frac{\partial^2}{\partial\lambda\,\partial\zeta}\,\frac{(\exp)_c}{\Omega_c W_c^2}\left(\frac{W_c}{Q_c}\right)^{i\xi_2}, \tag{59}$$

$$(\exp)_c=\left[\frac{1}{x}\,\frac{(xyv_1)^2-(p_c+\Lambda_c)^2}{(yv_1)^2-(p_c+\Omega_c+i\zeta)^2}\right]^{i\xi_c}, \tag{60}$$

$$\Lambda_c=\sqrt{(p_c^2-xy^2v_1^2)(1-x)+x(\Omega_c+i\zeta)^2}, \tag{61}$$

$$\Omega_c=\sqrt{(p_1t+i\lambda)^2y-v_1^2y(1-y)}, \tag{62}$$

$$W_c=(\tilde{\boldsymbol{\kappa}}+\boldsymbol{p}_2)^2-(\Lambda_c+i\varepsilon)^2, \tag{63}$$

$$Q_c=\tilde{\kappa}^2-(p_2+\Lambda_c+i\varepsilon)^2. \tag{64}$$

Here $\tilde{\boldsymbol{\kappa}}=xy\boldsymbol{v}_1-\boldsymbol{k}$, $\boldsymbol{v}_1=\boldsymbol{p}_1(1-t)$, $i\xi_c=i\eta/p_c=1/\sqrt{2+\varepsilon_1}=1/\sqrt{\omega-\varepsilon_2}$, and $p_c=\sqrt{2mE_c+i0}$ together with the energy E_c as given by Eq. (14). The functions $\tilde{F}_l$ in Eq. (57) are defined analogous to F_l in Eq. (50) with the replacement of f_l by $\tilde{f}_l$ $(l=1,2)$.

The amplitude corresponding to the Feynman diagram in Fig. 1(d) is determined by the following formulas:

$$\mathcal{A}_d=(4\pi)^2\alpha\,\frac{\sqrt{4\pi\alpha}}{\sqrt{2\omega}}\mathcal{N}\eta[(\mathbf{e}\cdot\boldsymbol{n}_1)\tilde{\Phi}_1+(\mathbf{e}\cdot\boldsymbol{n}_2)\tilde{\Phi}_2], \tag{65}$$

$$\tilde{\varphi}_1(t)=v_1\int_0^1 dx\int_0^1 dy\,\frac{\partial^2}{\partial\varepsilon\,\partial\lambda}\times\left\{1+\frac{2i\eta}{Q_d}[T+p_2+(\boldsymbol{n}_2\cdot\tilde{\boldsymbol{q}})]\right\}\frac{(\exp)_b}{\Lambda_b\Omega_c}\,\frac{xy}{W_d^2}\left(\frac{W_d}{Q_d}\right)^{i\xi_2}, \tag{66}$$

$$\tilde{\varphi}_2(t)=-i(\eta+ip_2)\int_0^1 dx\int_0^1 dy\,\frac{\partial^2}{\partial\varepsilon\,\partial\lambda}\,\frac{(\exp)_b}{\Lambda_b\Omega_c}\,\frac{x}{W_d^2}\left(\frac{W_d}{Q_d}\right)^{i\xi_2}, \tag{67}$$

$$W_d=(\tilde{\boldsymbol{q}}+\boldsymbol{p}_2)^2-T^2, \tag{68}$$

$$Q_d=\tilde{q}^2-(T+p_2)^2, \tag{69}$$

together with $T=\Lambda_b+\Omega_c+i\varepsilon$, $\tilde{\boldsymbol{q}}=y\boldsymbol{v}_1-x\boldsymbol{k}$, and $\boldsymbol{v}_1=\boldsymbol{p}_1(1-t)$. After the derivatives with respect to ζ, λ, and ε are performed, one should set $\zeta=\lambda=\eta$ and should take the limit $\varepsilon\to 0$ at the end. The function $\tilde{\Phi}_l$ in Eq. (65) looks similar to the function Φ_l in Eq. (54) with the substitution of φ_l by $\tilde{\varphi}_l$ $(l=1,2)$.

III. THE AMPLITUDE OF DOUBLE PHOTOIONIZATION IN THE ASYMPTOTIC DOMAIN OF PHOTON ENERGIES

The asymptotic domain of photon energies ω is characterized by the condition $I_{2K}\ll\omega\ll m$, where $\omega\sim\eta$. For those energies of a photon, one cannot neglect the spin-dependent part of the electron-photon interaction (1). The spin operator transforms the antisymmetric spin function into the symmetric triplet function. Therefore, the second term in Eq. (1) leads to transitions into the final triplet state. As a consequence, the symmetry of the spatial part of the wave function is also changed, i.e., it becomes antisymmetric. The expression for the transition amplitude into the triplet state looks as follows:

$$\mathcal{A}_\mu^t=\frac{i}{2m}\,\frac{\sqrt{4\pi\alpha}}{\sqrt{2\omega}}\times[\boldsymbol{k},\mathbf{e}]\cdot\langle\chi_{1\mu}\Psi_f^t|(\boldsymbol{\sigma}_1e^{i(\mathbf{k}\cdot\mathbf{r}_1)}+\boldsymbol{\sigma}_2e^{i(\mathbf{k}\cdot\mathbf{r}_2)})|\chi_0\Psi_i\rangle=(-1)^\mu\frac{i}{m}\,\frac{\sqrt{4\pi\alpha}}{\sqrt{2\omega}}[\boldsymbol{k},\mathbf{e}]_{-\mu}\langle\Psi_f^t|e^{i(\mathbf{k}\cdot\mathbf{r}_1)}|\Psi_i\rangle. \tag{70}$$

Here χ_0 is the spin function of the initial two-electron singlet state with zero total spin, $\chi_{1\mu}$ is the spin function of the final triplet state characterized by the total spin equal to 1 and the spin projection μ relative to a quantization axis. The spatial part of the wave function $\Psi_f^t\simeq\Psi_f^{(0)t}+\Psi_f^{(1)t}$ is now antisymmetric. In zeroth approximation, it looks as follows

$$\Psi_f^{(0)t}(\boldsymbol{r}_1,\boldsymbol{r}_2)=\frac{1}{\sqrt{2}}[\psi_{\boldsymbol{p}_1}(\boldsymbol{r}_1)\psi_{\boldsymbol{p}_2}(\boldsymbol{r}_2)-\psi_{\boldsymbol{p}_1}(\boldsymbol{r}_2)\psi_{\boldsymbol{p}_2}(\boldsymbol{r}_1)]. \tag{71}$$

The first-order correction $\Psi_f^{(1)t}$ to the wave function is defined by an expression similar to Eq. (7), where the function $\Psi_f^{(0)}$ is substituted by $\Psi_f^{(0)t}$.

Introducing the unit vector $\boldsymbol{n}_\gamma=\boldsymbol{k}/k$, we obtain

$$\mathcal{A}_\mu^t=\alpha Z\,\frac{ik}{\eta}\,\frac{\sqrt{4\pi\alpha}}{\sqrt{2\omega}}[\boldsymbol{n}_\gamma,\mathbf{e}]^\mu\langle\Psi_f^t|e^{i(\mathbf{k}\cdot\mathbf{r}_1)}|\Psi_i\rangle=\frac{ik}{2\eta}[\boldsymbol{n}_\gamma,\mathbf{e}]^\mu\mathcal{A}^t, \tag{72}$$

$$\mathcal{A}^t=\sqrt{2}[\mathcal{A}_a^t+\mathcal{A}_b^t-\mathcal{A}_c^t-\mathcal{A}_d^t]. \tag{73}$$

In Eq. (73), we write down explicitly the individual contributions for the amplitude of the singlet-triplet transition, which result for graphs in Figs. 1(a)–1(d), respectively. As can be seen from Eq. (70), in the case of a transition into the triplet state the photon vertex $\hat{\gamma}$ does not contain a factor $(\mathbf{e}\cdot\boldsymbol{f})$. Let us present the final formulas for the amplitudes

$$\mathcal{A}_a^t=(4\pi)^2\alpha\,\frac{\sqrt{4\pi\alpha}}{\sqrt{2\omega}}\mathcal{N}F,$$

$$F=-\frac{\eta}{2}\hat{\mathcal{I}}_{\xi_1}(t)\int_0^1 dx\int_0^1 dy\,\frac{\partial^3}{\partial\varepsilon\,\partial\lambda\,\partial\zeta}\,\frac{(\exp)_a}{\Lambda_a\Omega_a}\,\frac{1}{W_a}\left(\frac{W_a}{Q_a}\right)\Bigg|^{i\xi_2}_{\substack{\lambda=\eta\\ \zeta=\eta\\ \varepsilon\to 0}}, \tag{74}$$

$$\mathcal{A}_b^t=(4\pi)^2\alpha\frac{\sqrt{4\pi\alpha}}{\sqrt{2\omega}}\mathcal{N}\Phi,$$

$$\Phi=-\frac{\eta}{2}\hat{\mathcal{I}}_{\xi_1}(t)\int_0^1 dx\int_0^1 dy\,\frac{\partial^3}{\partial\varepsilon\,\partial\lambda\,\partial\eta}\,\frac{(\exp)_b}{\Lambda_b\Omega_b}\,\frac{1}{W_b}\left(\frac{W_b}{Q_b}\right)\Bigg|_{\substack{\lambda=\eta\\ \varepsilon\to 0}}^{i\xi_2}, \tag{75}$$

$$\mathcal{A}_c^t=(4\pi)^2\alpha\frac{\sqrt{4\pi\alpha}}{\sqrt{2\omega}}\mathcal{N}\tilde{F},$$

$$\tilde{F}=-\frac{\eta}{2}\hat{\mathcal{I}}_{\xi_1}(t)\int_0^1 dx\int_0^1 dy\,\frac{\partial^3}{\partial\varepsilon\,\partial\lambda\,\partial\zeta}\,\frac{(\exp)_c}{\Lambda_c\Omega_c}\,\frac{1}{W_c}\left(\frac{W_c}{Q_c}\right)\Bigg|_{\substack{\lambda=\eta\\ \zeta=\eta\\ \varepsilon\to 0}}^{i\xi_2}, \tag{76}$$

$$\mathcal{A}_d^t=(4\pi)^2\alpha\frac{\sqrt{4\pi\alpha}}{\sqrt{2\omega}}\mathcal{N}\tilde{\Phi},$$

$$\tilde{\Phi}=-\frac{\eta}{2}\hat{\mathcal{I}}_{\xi_1}(t)\int_0^1 dx\int_0^1 dy\,\frac{\partial^3}{\partial\varepsilon\,\partial\lambda\,\partial\eta}\,\frac{(\exp)_b}{\Lambda_b\Omega_c}\,\frac{1}{W_d}\left(\frac{W_d}{Q_d}\right)\Bigg|_{\substack{\lambda=\eta\\ \varepsilon\to 0}}^{i\xi_2}. \tag{77}$$

All quantities are similar to those defined in Sec. II. The partial derivative $\partial/\partial\eta$ does not act on ξ_b and ξ_2. The formulas for the transition into the final singlet state, which were derived in Sec. II in the dipole energy regime, are also valid in the asymptotical domain, because they are derived without performing an expansion with respect to the photon momentum.

IV. THE MAGNETIC DIPOLE TRANSITION AMPLITUDE VANISHES

In Secs. II and III, we have derived nonrelativistic expressions for amplitudes of the double *K*-shell photoeffect with a complete dependence upon the photon momentum $\boldsymbol{k}$. In the electric dipole approximation, one sets $k=0$ in Eq. (1). Going beyond the dipole approximation means to retain at least the first $\boldsymbol{k}$-dependent term in the expansion $\exp(i\boldsymbol{k}\cdot\boldsymbol{r})\simeq 1+i(\boldsymbol{k}\cdot\boldsymbol{r})-\cdots$, which has a relative smallness of the order of k/η in the near-threshold domain. The $i(\boldsymbol{k}\cdot\boldsymbol{r})$ term gives rise to magnetic dipole and electric quadrupole transition amplitudes. Due to the interference between the electric dipole and the electric quadrupole amplitudes in differential double-photoionization cross sections, the nondipole effect turns out to be of the same order as k/η. In the case of the single photoeffect the magnetic dipole amplitude is known to give a vanishing contribution within the framework of the nonrelativistic description, due to the orthogonality of bound and continuum wave functions [37–39]. Below we shall show that a similar result is also valid for the double *K*-shell photoionization.

The magnetic dipole transition is caused by the following interaction [37]:

$$\hat{\gamma}=\frac{i}{2m}\frac{\sqrt{4\pi\alpha}}{\sqrt{2\omega}}([\boldsymbol{k},\mathbf{e}]\cdot(\hat{\boldsymbol{L}}+\boldsymbol{\sigma})), \tag{78}$$

where $\hat{\boldsymbol{L}}=[\boldsymbol{r},\hat{\boldsymbol{p}}]$ is the operator of the orbital angular momentum. For convenience we shall work in the coordinate representation. Assuming that the x and y axes are directed along the vectors $\boldsymbol{k}$ and $\mathbf{e}$, respectively, the operator $\hat{\boldsymbol{L}}$ preserves only its component $\hat{L}_z$ relative to the z axis. Then the orbital part of the magnetic dipole transition amplitude corresponding to the graph in Fig. 1(a) reads

$$\frac{ik}{2m}\frac{\sqrt{4\pi\alpha}}{\sqrt{2\omega}}\int d\boldsymbol{r}d\boldsymbol{r}_1d\boldsymbol{r}_2\psi_{\boldsymbol{p}_1}^*(\boldsymbol{r})\hat{L}_zG_C(\boldsymbol{r},\boldsymbol{r}_1;E_a)\times\frac{1}{r_{12}}\psi_{\boldsymbol{p}_2}^*(\boldsymbol{r}_2)\psi_{1s}(\boldsymbol{r}_1)\psi_{1s}(\boldsymbol{r}_2). \tag{79}$$

The wave function of the ejected electron can be written in terms of the partial-wave decomposition [40],

$$\psi_{\boldsymbol{p}}(\boldsymbol{r})=\frac{2\pi}{p}\sum_{l=0}^{\infty}i^le^{-i\delta_l(p)}R_{pl}(r)\sum_m Y_{lm}\left(\frac{\boldsymbol{r}}{r}\right)Y_{lm}^*\left(\frac{\boldsymbol{p}}{p}\right), \tag{80}$$

where $\delta_l(p)$ are the phase shifts of the radial functions R_{pl}. The latter are orthogonal and normalized according to

$$\int_0^\infty dr r^2R_{p'l}(r)R_{pl}(r)=2\pi\delta(p'-p). \tag{81}$$

The wave functions (80) are normalized according to the condition

$$\int d\boldsymbol{r}\psi_{\boldsymbol{p}'}^*(\boldsymbol{r})\psi_{\boldsymbol{p}}(\boldsymbol{r})=(2\pi)^3\delta(\boldsymbol{p}'-\boldsymbol{p}), \tag{82}$$

which is usual for the continuous spectrum. The spherical functions $Y_{lm}(\boldsymbol{n})$ are eigenfunctions of the operator $\hat{L}_z$.

The Coulomb Green's function reads

$$G_C(\boldsymbol{r},\boldsymbol{r}';E_a)=\int\frac{d\boldsymbol{p}}{(2\pi)^3}\frac{\psi_{\boldsymbol{p}}(\boldsymbol{r})\psi_{\boldsymbol{p}}^*(\boldsymbol{r}')}{E_a-E_p} \tag{83}$$

$$=\int_0^\infty\frac{dp}{2\pi}\sum_{l=0}^{\infty}\frac{R_{pl}(r)R_{pl}(r')}{E_a-E_p}\times\sum_m Y_{lm}\left(\frac{\boldsymbol{r}}{r}\right)Y_{lm}^*\left(\frac{\boldsymbol{r}'}{r'}\right), \tag{84}$$

where the summation over the discrete spectrum is also assumed. The partial-wave decomposition of Green's function $1/r_{12}$ for the scalar Laplace equation is given by

$$\frac{1}{r_{12}}=4\pi\sum_{l=0}^{\infty}\frac{1}{(2l+1)}\frac{r_<^l}{r_>^{l+1}}\sum_m Y_{lm}\left(\frac{\boldsymbol{r}_1}{r_1}\right)Y_{lm}^*\left(\frac{\boldsymbol{r}_2}{r_2}\right), \tag{85}$$

where $r_<=\min\{r_1,r_2\}$ and $r_>=\max\{r_1,r_2\}$.

With the aid of the normalization condition (81) and the expansions (80), (84), and (85), the expression (79) takes the form

$$\frac{ik}{m}\frac{\sqrt{4\pi\alpha}}{\sqrt{2\omega}}\frac{(2\pi)^3}{p_1p_2}\sum_{l=1}^{\infty}\frac{(-1)^l}{(2l+1)} \times e^{i[\delta_l(p_1)+\delta_l(p_2)]}\frac{I_l(p_1,p_2)}{E_a-E_{p_1}}\sum_{\mu}\mu Y_{l\mu}\left(\frac{\boldsymbol{p}_1}{p_1}\right)Y^*_{l\mu}\left(\frac{\boldsymbol{p}_2}{p_2}\right). \tag{86}$$

The radial integral $I_l(p_1,p_2)$, which is defined as

$$I_l(p_1,p_2)=\int_0^{\infty}dr_1r_1^2dr_2r_2^2R_{p_1l}(r_1)R_{p_2l}(r_2) \times\frac{r_<^l}{r_>^{l+1}}\psi_{1s}(r_1)\psi_{1s}(r_2), \tag{87}$$

is symmetrical, i.e., $I_l(p_1,p_2)=I_l(p_2,p_1)$.

The orbital part of the magnetic dipole transition amplitude corresponding to the exchange diagram in Fig. 1(c) is derived in a similar manner. It reads

$$\frac{ik}{m}\frac{\sqrt{4\pi\alpha}}{\sqrt{2\omega}}\frac{(2\pi)^3}{p_1p_2}\sum_{l=1}^{\infty}\frac{(-1)^l}{(2l+1)} \times e^{i[\delta_l(p_1)+\delta_l(p_2)]}\frac{I_l(p_2,p_1)}{E_c-E_{p_2}}\sum_{\mu}\mu Y_{l\mu}\left(\frac{\boldsymbol{p}_2}{p_2}\right)Y^*_{l\mu}\left(\frac{\boldsymbol{p}_1}{p_1}\right). \tag{88}$$

Taking into account that $E_a-E_{p_1}=E_c-E_{p_2}=-\omega$ and using the following property of the spherical functions $Y^*_{lm}=(-1)^mY_{l,-m}$, one can see that the amplitudes (86) and (88) cancel each other. The cancellation of amplitudes describing the absorption of the right- and left-polarized photons, which correspond to the matrix elements of the operators $\hat{L}_{\pm}=\hat{L}_x\pm i\hat{L}_y$, can be proven in a similar manner. The orbital part of the magnetic dipole contribution vanishes also in the separate graphs in Figs. 1(b) and 1(d). This is easy to verify, because the operator $\hat{\boldsymbol{L}}$ of the orbital angular momentum results in differentiations with respect to angles, while the ground-state function ψ_{1s} is independent of angles.

Let us consider the magnetic-dipole transition amplitude, which is caused by the spin-dependent term of the interaction (78). Since the matrix element $F(\boldsymbol{p}_2,\boldsymbol{f})$ is the same in amplitudes corresponding to graphs in Figs. 1(a) and 1(b) [see Eqs. (18) and (38)], it is sufficient to evaluate the following matrix element:

$$\frac{i}{2m}\frac{\sqrt{4\pi\alpha}}{\sqrt{2\omega}}([\boldsymbol{k},\mathbf{e}]\cdot\boldsymbol{\sigma})\int\frac{d\boldsymbol{f}'}{(2\pi)^3}\frac{d\boldsymbol{f}_1}{(2\pi)^3}\langle\psi_{\boldsymbol{p}_1}|\boldsymbol{f}'\rangle \times\langle\boldsymbol{f}'|G_C(E_a)|\boldsymbol{f}_1\rangle\langle\boldsymbol{f}_1+\boldsymbol{f}|\psi_{1s}\rangle. \tag{89}$$

With the aid of the representation of Green's function analogous to Eq. (83) and the normalization condition (82), the expression (89) takes the form

$$\frac{i}{2m}\frac{\sqrt{4\pi\alpha}}{\sqrt{2\omega}}([\boldsymbol{k},\mathbf{e}]\cdot\boldsymbol{\sigma})\int\frac{d\boldsymbol{f}_1}{(2\pi)^3}\frac{\langle\psi_{\boldsymbol{p}_1}|\boldsymbol{f}_1\rangle}{E_a-E_{p_1}}\langle\boldsymbol{f}_1+\boldsymbol{f}|\psi_{1s}\rangle. \tag{90}$$

The spin-dependent magnetic dipole contribution corresponding to the graph in Fig. 1(b) can be written as

$$\frac{i}{2m}\frac{\sqrt{4\pi\alpha}}{\sqrt{2\omega}}([\boldsymbol{k},\mathbf{e}]\cdot\boldsymbol{\sigma})\int\frac{d\boldsymbol{f}'}{(2\pi)^3}\frac{\langle\psi_{\boldsymbol{p}_1}|\boldsymbol{f}'-\boldsymbol{f}\rangle}{E_b-E_{1s}}\langle\boldsymbol{f}'|\psi_{1s}\rangle. \tag{91}$$

Taking into account that $E_a-E_{p_1}=E_{1s}-E_b=-\omega$, one can see that the contributions given by Eqs. (90) and (91) cancel each other. The same occurs for the exchange diagrams in Figs. 1(c) and 1(d), respectively.

Concluding, we have shown that the magnetic dipole transition amplitude describing the double *K*-shell photoionization vanishes within the framework of the nonrelativistic consideration. In addition, since the spin operator changes the symmetry of spin functions in the initial and final electron states, the orbital contribution does not interfere with that corresponding to the spin-dependent term in Eq. (1). As a result, the singlet-triplet transition turns out to be suppressed by a factor of about k^4/η^4 in cross sections of the process in the near-threshold domain. The derivation presented can be easily generalized for any singlet $^1S_0$ state.

V. DIFFERENTIAL AND TOTAL CROSS SECTIONS FOR THE DOUBLE PHOTOIONIZATION

The basic quantity for describing the process under investigation is the fivefold differential cross section $d^5\sigma^{++}$, from which all the angular and energy distributions for photoelectrons can be derived. The cross sections should be summed over the final states of the system:

$$d^5\sigma^{++}=2\pi\left\{|\mathcal{A}|^2+\sum_{\mu}|\mathcal{A}^t_{\mu}|^2\right\}\frac{d\boldsymbol{p}_1}{(2\pi)^3} \times\frac{d\boldsymbol{p}_2}{(2\pi)^3}\delta(E_{p_1}+E_{p_2}+I_{2K}-\omega) =\frac{m^2p_1p_2}{(2\pi)^5}\left\{|\mathcal{A}|^2+\frac{k^2}{4\eta^2}|\mathcal{A}^t|^2\right\}d\Omega_1d\Omega_2dE_{p_2}, \tag{92}$$

where $\mathcal{A}$ and $\mathcal{A}^t$ are defined by Eqs. (8) and (73), respectively. It should be noted that the second term in Eq. (92) is independent of the photon polarization.

For convenience we introduce dimensionless amplitudes, $\mathcal{L}$ and $\mathcal{L}^t$, according to the following relation:

$$|\mathcal{A}|^2+\frac{k^2}{4\eta^2}|\mathcal{A}^t|^2=(4\pi)^5\frac{\alpha^3\mathcal{N}^2}{\omega\eta^{12}}\left\{|\mathcal{L}|^2+\frac{k^2}{4}|\mathcal{L}^t|^2\right\}. \tag{93}$$

All momenta on the right-hand side of Eq. (93) are supposed to be expressed in units of $\eta=m\alpha Z$. For example, the dimensionless momentum of a photon is $k=k/\eta$. Introducing as well dimensionless energies for the incoming photon, $\varepsilon_\gamma=\omega/I$, and for both outgoing electrons, $\varepsilon_l=E_{p_l}/I$ $(l=1,2)$, where $I=\eta^2/(2m)$, one obtains

$$d^5\sigma^{++}=\frac{2^7\alpha a_0^2}{Z^4\varepsilon_\gamma\chi}\left\{|\mathcal{L}|^2+\frac{k^2}{4}|\mathcal{L}^t|^2\right\}d\Omega_1 d\Omega_2 d\varepsilon_2. \tag{94}$$

Here $\mathcal{L}=(\mathbf{e}\cdot\boldsymbol{n}_1)\mathcal{F}_1+(\mathbf{e}\cdot\boldsymbol{n}_2)\mathcal{F}_2$, $\mathcal{F}_l=F_l+\Phi_l+\tilde{F}_l+\tilde{\Phi}_l$ $(l=1,2)$, $\mathcal{L}^t=F+\Phi-\tilde{F}-\tilde{\Phi}$, and $a_0=1/(m\alpha)$ denotes the Bohr radius. In Eq. (94), the factor χ is given by $\chi=[1-\exp(-2\pi\tau_1)][1-\exp(-2\pi\tau_2)]$, where $\tau_1=1/\sqrt{\varepsilon_1}=1/\sqrt{\varepsilon_\gamma-\varepsilon_2-2}$ and $\tau_2=1/\sqrt{\varepsilon_2}$. It is interesting to note that the amplitudes $\mathcal{L}$ and $\mathcal{L}^t$ being expressed in terms of the dimensionless quantities, such as energies and momenta, now depend on the nuclear charge number Z via the photon momentum $k=\alpha Z\varepsilon_\gamma/2$, which serves as a quantitative measure of the nondipolarity. The latter is due to the mutual interplay between two input parameters, Z and ε_γ.

In the following, we shall restrict to the dipole domain of photon energies, where the contribution of the second term in brackets of Eq. (94) can be neglected. However, we keep a complete dependence upon the vector $\boldsymbol{k}$ in the amplitude $\mathcal{L}$. This allows us to go beyond the dipole approximation and to calculate a contribution to differential and total cross sections of the process arising from the photon momentum in the dipole regime. In the case of unpolarized photons, the averaging of the cross section (94) over the polarizations of the incoming photon results in a replacement of $|\mathcal{L}|^2$ by

$$\overline{|\mathcal{L}|^2}=\tfrac{1}{2}\{|\mathcal{F}_1|^2\sin^2\theta_1+|\mathcal{F}_2|^2\sin^2\theta_2+2\mathrm{Re}(\mathcal{F}_1\mathcal{F}_2^*)\times(\cos\theta_{12}-\cos\theta_1\cos\theta_2)\}, \tag{95}$$

where θ_i are angles between the vectors $\boldsymbol{k}$ and $\boldsymbol{p}_i$ $(i=1,2)$. The angle θ_{12} is that enclosed by the vectors $\boldsymbol{p}_1$ and $\boldsymbol{p}_2$.

The energy distribution of the emitted electrons can be found after integration of Eq. (94) over the angles. The dependence of the amplitudes $\mathcal{F}_l$ $(l=1,2)$ upon the azimuthal angle results only through the function $\cos\theta_{12}=\cos\theta_1\cos\theta_2+\sin\theta_1\sin\theta_2\cos(\varphi_2-\varphi_1)$. One may introduce a relative angle $\varphi=\varphi_2-\varphi_1$ instead of the angle φ_2. This eliminates all dependence on φ_1 and leads to a factor 2π after the angular integration. Then $d\Omega_1 d\Omega_2=2\pi\sin\theta_1 d\theta_1\sin\theta_2 d\theta_2 d\varphi$. The angle φ varies from 0 to 2π. However, it is easy to verify that the relation

$$\int_0^{2\pi}d\varphi f(\cos\theta_{12})=2\int_0^{\pi}d\varphi f(\cos\theta_{12}) \tag{96}$$

holds for any function $f(\cos\theta_{12})$. Accordingly, the energy distribution simplifies to

$$\frac{d\sigma^{++}}{d\varepsilon_2}=\frac{2^{10}\pi\sigma_0}{3Z^4\varepsilon_\gamma}G(\varepsilon_2,\varepsilon_\gamma;k), \tag{97}$$

$$G(\varepsilon_2,\varepsilon_\gamma;k)=\frac{3}{4\pi\chi}\int_0^\pi d\theta_1\sin\theta_1\int_0^\pi d\theta_2\sin\theta_2\int_0^\pi d\varphi\times\{|\mathcal{F}_1|^2\sin^2\theta_1+|\mathcal{F}_2|^2\sin^2\theta_2+2\mathrm{Re}(\mathcal{F}_1\mathcal{F}_2^*)\sin\theta_1\sin\theta_2\cos\varphi\}, \tag{98}$$

where $\sigma_0=\alpha\pi a_0^2$. Due to a complicated dependence of the amplitudes upon the angles, the further integrations in Eq. (98) can be performed only numerically.

We denote the total energy of both outgoing electrons as $\varepsilon=\varepsilon_1+\varepsilon_2=\varepsilon_\gamma-2$. The double-photoionization threshold corresponds to the photon energy $\varepsilon_\gamma^{\mathrm{th}}=2$. To obtain the total cross section, Eq. (97) should be further integrated over the energy ε_2 from 0 to $\varepsilon/2$ (or, equivalently, over the energy ε_1 from $\varepsilon/2$ to ε):

$$\sigma^{++}(\varepsilon_\gamma;k)=\sigma_0\frac{2^{10}\pi}{3Z^4}Q(\varepsilon_\gamma;k), \tag{99}$$

$$Q(\varepsilon_\gamma;k)=\frac{1}{\varepsilon_\gamma}\int_0^{\varepsilon/2}d\varepsilon_2 G(\varepsilon_2,\varepsilon_\gamma;k). \tag{100}$$

In the dipole approximation $(k=0)$, the amplitudes $\mathcal{F}_1$ and $\mathcal{F}_2$ depend only on the angle θ_{12} via $\cos\theta_{12}$. In this case the expression (98) can be further simplified to

$$G(\varepsilon_2,\varepsilon_\gamma;0)=\int_0^\pi d\theta_{12}\sin\theta_{12}\{|\mathcal{F}_1|^2+|\mathcal{F}_2|^2+2\mathrm{Re}(\mathcal{F}_1\mathcal{F}_2^*)\cos\theta_{12}\}. \tag{101}$$

Moreover, the quantity $Q(\varepsilon_\gamma;0)$ becomes independent of Z. The same holds true for the whole helium isoelectronic sequence. Accordingly, up to leading order of the expansion over $1/Z$ the product $Z^4\sigma^{++}$ does not depend on Z within the dipole approximation only. The corresponding expression for the cross section σ^+ of the single K-shell photoionization derived without taking into account the electron-electron interaction is well known [31]:

$$\sigma^+(\varepsilon_\gamma;0)=\sigma_0\frac{2^{10}\pi}{3Z^2}H(\varepsilon_\gamma;0), \tag{102}$$

$$H(\varepsilon_\gamma;0)=\frac{1}{\varepsilon_\gamma^4}\frac{\exp(-4\tau\cot^{-1}\tau)}{[1-\exp(-2\pi\tau)]}, \tag{103}$$

where $\tau=1/\sqrt{\varepsilon_\gamma-1}$. The rigorous QED calculations of cross sections describing the single photoionization and the single ionization with excitation in the next-to-leading order of perturbation theory in $1/Z$ are presently not available. The ratio R of double-to-single ionization cross sections, which is usually measured experimentally, is given by

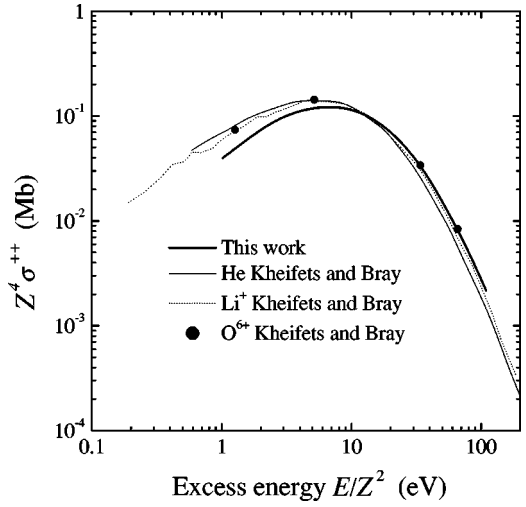

FIG. 2. The universal quantity $Z^4\sigma^{++}$ is calculated in dipole approximation as a function of the scaled excess energy $E=E_{p_1}+E_{p_2}$. Numerical results for He, Li^+, and O^{6+} have been obtained by Kheifets and Bray within the framework of the convergent close-coupling formalism using the 20-parameter Hylleraas ground-state wave functions [19].

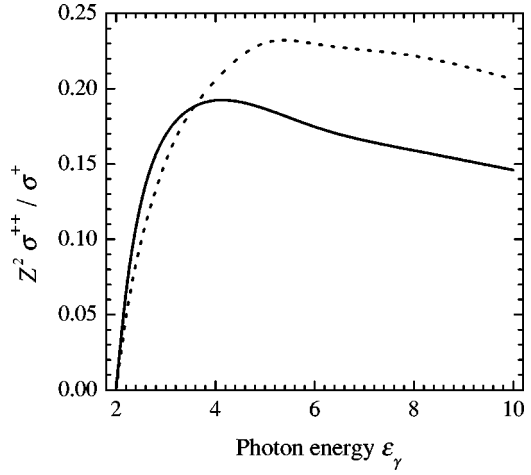

FIG. 3. Different contributions to the universal ratio $Z^2R(\varepsilon_\gamma)$ of double-to-single photoionization cross sections calculated in Coulomb gauge for $k=0$ according to Eq. (104). Dashed line, contribution due to the Feynman diagrams in Figs. 1(a) and 1(c) only; solid line, total contribution of all diagrams.

$$R(\varepsilon_\gamma)=\frac{\sigma^{++}(\varepsilon_\gamma;0)}{\sigma^{+}(\varepsilon_\gamma;0)}=\frac{1}{Z^2}\frac{Q(\varepsilon_\gamma;0)}{H(\varepsilon_\gamma;0)}. \qquad (104)$$

The universal scaling for $Z^2R(\varepsilon_\gamma)$ appears again in leading order of the perturbation theory with respect to the parameter $1/Z$, if one sets $k=0$ only.

VI. NUMERICAL RESULTS AND DISCUSSION

In the evaluation of matrix elements, differentiations involved have been performed analytically with the aid of the computer algebra system MATHEMATICA. For subsequent numerical integrations, the standard Gauss-Kronrod method has been employed. To achieve stable results, some of the integrals over the interval [0,1] were performed along different contours, such as ellipse, semiellipse, or semicircle, in the complex plane. In the case of equal electron momenta, the contributions from both direct and exchange Feynman graphs coincide with each other, although their functional dependences seem to be different. Assuming $p_1=p_2$, we made these additional cross-checks of the quality of the numerical integrations.

In Fig. 2, we compare the universal quantity $Z^4\sigma^{++}$ obtained in dipole approximation with numerical results of Ref. [19]. As can be seen, the curves lie relatively close to each other, although they are not identical. The contributions to σ^{++} due to the two-photon exchange graphs turn out to be relatively small. It should be noted that the curves for $Z^4\sigma^{++}$ calculated by Kheifets and Bray [19] show a slight dependence on Z even in the dipole approximation. This occurs because of the necessity to take into account next-to-leading order terms (in the sense of perturbation theory) and in order to adjust the threshold energies for each particular ion. In Fig. 3, the universal ratio $Z^2R(\varepsilon_\gamma)$ is depicted, which is valid for moderate values of $Z\geqslant 2$ [41]. Accounting for the electron-electron interaction to the final state results in significant corrections to the total cross section of the double photoionization. However, the individual contributions of each diagram are gauge dependent. Note also that the maxima of the curves $Z^4\sigma^{++}$ and $Z^2\sigma^{++}/\sigma^{+}$ peak at different values of the photon energy ε_γ. The curve $Z^4\sigma^{++}$ reaches its maximum at about $\varepsilon_\gamma\simeq 2.5$, while the ratio $Z^2\sigma^{++}/\sigma^{+}$ becomes extremal at about $\varepsilon_\gamma\simeq 4$ (see Fig. 3).

In Ref. [41], our numerical results for the ratio R given by Eq. (104) have been compared with most recent measurements performed for the ratio in helium [4–6]. Accounting for electron-electron interaction corrections to σ^{+} as well as accounting for the single photoionization with excitation turn out to be more essential than accounting for two-photon exchange graphs to σ^{++}. The fast convergence of the perturbation theory over $1/Z$ in entire nonrelativistic domain is connected with the smallness of coefficients of the expansion, which accelerates the convergence for any small value of $Z\geqslant 2$. One can also mention here similar example from QCD, where the expansion over $1/N_c$ for the number of quark colors $N_c=3$ is known to converge by an order of magnitude due to appearance of the additional factor $1/\pi$ [42].

In Fig. 4, the energy distributions are presented for heliumlike molybdenum with respect to the energy of one of the outgoing electrons, without distinguishing between fast and slow particles. In each event of the double photoionization, both electrons, the fast and the slow one, leave an atom pairwise. In virtue of the energy-conservation law, the excess energy ε is fixed by the energy ε_γ of the incident photon, taking into account the reduction by the ionization energy. Furthermore, the number of slow electrons is equal to the number of fast electrons. These two circumstances lead to the symmetry of the energy distributions relative to the center point $\varepsilon/2$ of the energy interval. Since the double-photoionization cross section is quite close to its maximum

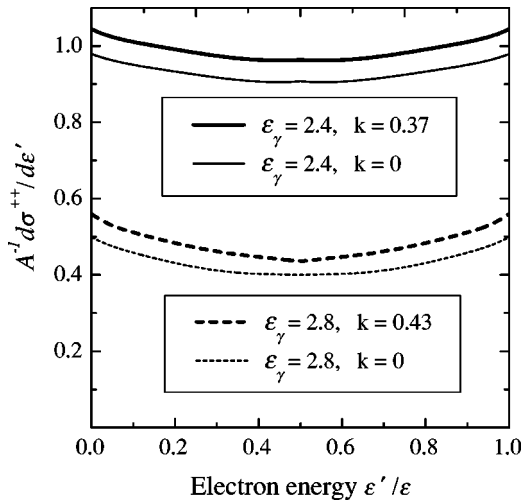

FIG. 4. The energy distributions are calculated for heliumlike molybdenum with respect to the energy of one of the ejected electrons. The energy parameter ε' is either ε_1 or ε_2, taking into account that one does not distinguish between fast and slow electrons. The curves are obtained within the dipole approximation and beyond. The normalization coefficient is given by $A=\sigma_0/Z^4$, where $\sigma_0=\alpha\pi a_0^2=0.642$ Mb with $a_0=1/(m\alpha)$ being the Bohr radius.

at the photon energy $\varepsilon_\gamma=2.4$, the energy distribution of the emitted electrons lies in this case higher than that at $\varepsilon_\gamma=2.8$ (see Fig. 4). In addition, the energy dependence turns out to be rather weak in the vicinity of the double-photoionization threshold. The comparable contributions to the cross section arise from the emission of electrons with arbitrary energy sharing. However, increasing the photon energy ε_γ further, it becomes distributed very nonuniformly among the outgoing electrons [43], although employment of the dipole approximation may be still adequate.

In Ref. [43], we have presented the angular distributions

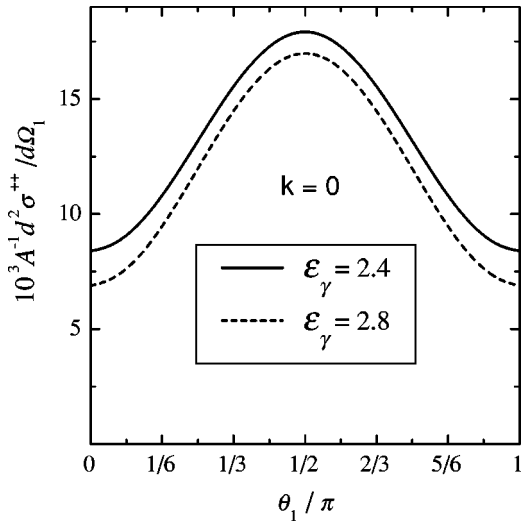

FIG. 5. The angular distributions of fast electrons are calculated for heliumlike molybdenum within the dipole approximation. The normalization factor A is the same as in Fig. 4. The angle θ_1 is that between the vectors $\boldsymbol{k}$ and $\boldsymbol{p}_1$, and $d\Omega_1$ is the solid angle of fast electrons.

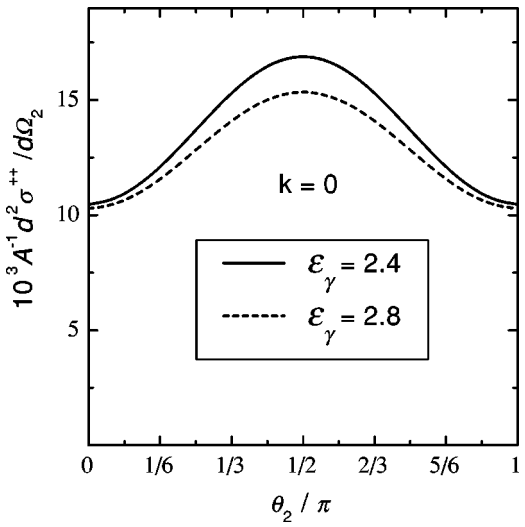

FIG. 6. The angular distributions of slow electrons are calculated for heliumlike molybdenum within the dipole approximation. The angle θ_2 is that between the vectors $\boldsymbol{k}$ and $\boldsymbol{p}_2$, and $d\Omega_2$ is the solid angle of slow electrons. The normalization factor A is the same as in Fig. 4.

for the fast and slow electrons, calculated for heliumlike neon and calcium with taking into account the complete dependence upon the photon momentum corresponding to the energy $\varepsilon_\gamma=8$. The results are compared with those obtained within the dipole approximation. As a limiting case, we have also calculated the angular distributions for heliumlike molybdenum [see Figs. 5–8]. The photon energies have been chosen to be $\varepsilon_\gamma=2.4$ and $\varepsilon_\gamma=2.8$, which correspond to photon momenta $k=0.37$ and $k=0.43$, respectively. Although the accuracy of our calculations in Mo^{40+} can be estimated to be of about 10% due to relativistic corrections omitted in

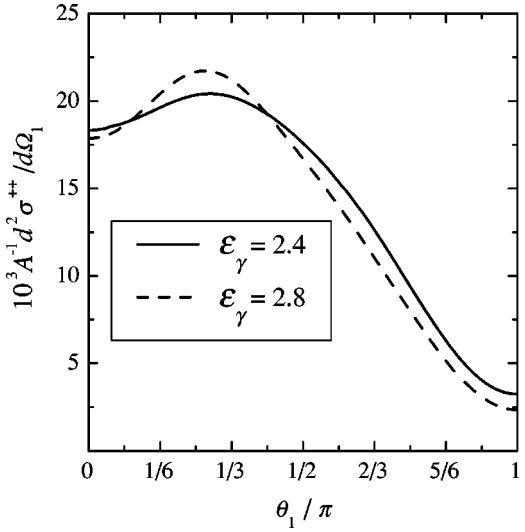

FIG. 7. The angular distributions of fast electrons are calculated for heliumlike molybdenum beyond the dipole approximation. The momentum k of an incoming photon is determined by the chosen photon energy $\varepsilon_\gamma=2.4$ or $\varepsilon_\gamma=2.8$ and the nuclear charge number $Z=42$ according to $k=\alpha Z\varepsilon_\gamma/2$. The notations are the same as in Fig. 5.

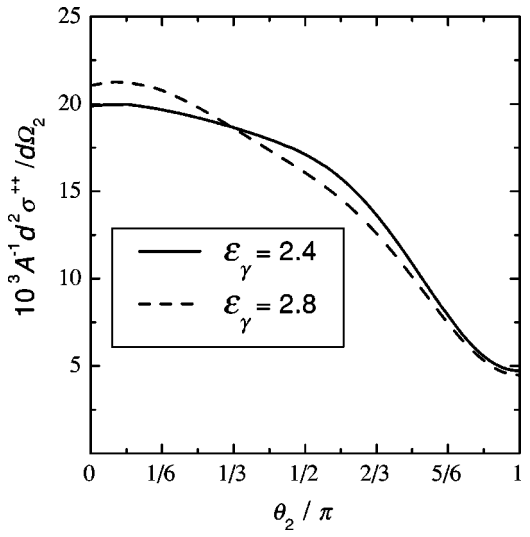

FIG. 8. The angular distributions of slow electrons are calculated for heliumlike molybdenum beyond the dipole approximation. The notations are the same as in Fig. 6.

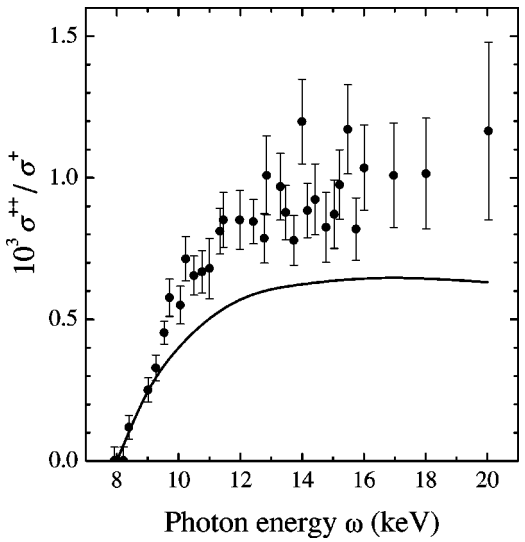

FIG. 9. A comparison between the theoretical and experimental ratios of double-to-single *K*-shell photoionization cross sections in neutral calcium. Experimental data are taken from Oura *et al.* [14].

the present investigation, the nondipole effects become here much more pronounced already in the vicinity of the double-ionization threshold.

Within the dipole approximation, the angular distributions for both ejected electrons are symmetric with respect to the plane perpendicular to the photon beam. Although the photon momentum $\boldsymbol{k}$ is completely neglected within the dipole approximation, the polarization vector **e** defines a distinguishing direction for the preferred ejection of electrons. The curves become asymmetrical, if one accounts for a nonzero momentum of the incident photon. The nondipole terms give rise to positive (negative) contributions to the cross section for the electron emission in forward (backward) direction. Accordingly, both electrons are preferably ejected in the forward hemisphere ($\theta_1, \theta_2 < \pi/2$). Moreover, in double photoionization, the electrons can leave an atom in forward and backward directions relative to the incident photon. Nevertheless, a simultaneous ejection of both electrons along the direction of the photon beam ($\theta_1 = \theta_2 = 0$, or $\theta_1 = \theta_2 = \pi$, or $\theta_1 = 0$ and $\theta_2 = \pi$, or $\theta_1 = \pi$ and $\theta_2 = 0$) is forbidden. This can be seen directly from the relation (95), which vanishes in these particular cases. Note that for the single photoeffect, the electron emission in forward and backward directions cannot occur within the framework of the nonrelativistic description.

Considering double *K*-shell photoionization in neutral atoms, the wave functions and Green's functions possess essentially a non-Coulomb behavior. Accordingly, numerical calculations require the use of the Hartree-Fock method already in zeroth approximation. Formally, the screening effect can be simulated by replacing the true nuclear charge number Z in Eq. (104) by an effective value Z_{eff}. The latter can be defined by equating the experimental potential I^{expt} for single *K*-shell ionization and the effective one, that is, $I^{\mathrm{expt}} = m(\alpha Z_{\mathrm{eff}})^2/2$. In Table I, we present a comparison of our predictions for neutral atoms with available experimental data. The significant disagreement for the nickel atom seems to be just due to high uncertainties of the results, both theo-

TABLE I. For various neutral atoms, the nuclear charge numbers Z, the experimental energies ω of an incident photon, the experimental potentials I^{expt} for single *K*-shell ionization [44], dimensionless photon energies ε_γ, effective values Z_{eff} for the nuclear charge, and the theoretical and experimental ratios $R(\varepsilon_\gamma)$ of double-to-single *K*-shell ionization cross sections are tabulated. The photon energies ω are calibrated in units of the experimental ionization potentials I^{expt}. The theoretical ratios $R(\varepsilon_\gamma)$ are calculated using the effective values Z_{eff} according to Eq. (104).

Neutral atom	Z	ω (keV)	I^{expt} (keV)	ε_γ	Z_{eff}	$R(\varepsilon_\gamma)$ This work	$R(\varepsilon_\gamma)$ Experiment	Reference
Ne	10	5	0.87	5.75	8.0	0.28×10^{-2}	$0.32(4)\times10^{-2}$	[13]
Ti	22	17.4	4.97	3.50	19.11	0.51×10^{-3}	0.53×10^{-3}	[10]
Cr	24	17.4	5.99	2.90	20.98	0.37×10^{-3}	0.38×10^{-3}	[10]
Fe	26	17.4	7.12	2.44	22.88	0.23×10^{-3}	0.24×10^{-3}	[10]
Ni	28	17.4	8.34	2.09	24.76	0.51×10^{-4}	1.1×10^{-4}	[10]
Cu	29	20	8.99	2.22	25.70	1.1×10^{-4}	$1.3(3)\times10^{-4}$	[12]
Mo	42	50	20.01	2.50	38.35	0.87×10^{-4}	$3.4(6)\times10^{-4}$	[11]

retical and experimental. The ratio $R(\varepsilon_\gamma)$ here is extremely sensitive to the photon energy, because the latter is very close to the threshold energy. It should be noted that the experimental uncertainty in Ni has been estimated to be of about 30% [10]. In the case of molybdenum, the deviation may be connected with relativistic effects, for example, with the spin-orbit interaction, which have been neglected in the present consideration. Another possible explanation might be higher error bars rather than those quoted in Ref. [11]. From the comparison with the measurements performed on Ca, Ti, and V in Ref. [14] one can see that theoretical calculations underestimate the corresponding experimental curves. The discrepancies exceed the experimental uncertainties and increase up to about 30% beyond the maxima of photoionization double-to-single ratios. The reason for this so far is unclear. The satisfactory agreement has been found only in the case of Ca just above the threshold (see Fig. 9).

Concluding, we have investigated the double *K*-shell photoionization for heliumlike ions and neutral atoms with moderate Z values, taking into account the leading orders of $1/Z$ and αZ expansions. QED perturbation theory with respect to the parameter $1/Z$ shows a fast convergence in the entire nonrelativistic domain for $Z \geqslant 2$. The electric dipole approximation can become inadequate for the description of angular distributions in a quite wide domain of nonrelativistic photon energies. Because of a nonzero photon momentum, the number of electrons leaving an atom in the forward direction with respect to the photon beam becomes larger than the number of electrons ejected in backward direction. Going beyond the leading-order consideration requires a rigorous QED treatment.

ACKNOWLEDGMENTS

We thank S.H. Southworth and M. Oura for useful communications. A.I.M. is grateful to the Dresden University of Technology for its hospitality and to DFG for financial support. G.S. and G.P. acknowledge financial support from BMBF, DFG, and GSI. A.I.M., I.A.M., A.N.M., and A.V.N. are supported by RFBR (Grants No. 01-02-17246 and No. 00-15-96610). A.V.N. acknowledges support from the Alexander von Humboldt Foundation.

[1] M. Ya. Amusia, *Atomic Photoeffect* (Plenum, New York, 1990).
[2] J.H. McGuire, N. Berrah, R.J. Bartlett, J.A.R. Samson, J.A. Tanis, C.L. Cocke, and A.S. Schlachter, J. Phys. B **28**, 913 (1995).
[3] J.S. Briggs and V. Schmidt, J. Phys. B **33**, R1 (2000).
[4] J.C. Levin, G.B. Armen, and I.A. Sellin, Phys. Rev. Lett. **76**, 1220 (1996).
[5] R. Dörner, T. Vogt, V. Mergel, H. Khemliche, S. Kravis, C.L. Cocke, J. Ullrich, M. Unverzagt, L. Spielberger, M. Damrau, O. Jagutzki, I. Ali, B. Weaver, K. Ullmann, C.C. Hsu, M. Jung, E.P. Kanter, B. Sonntag, M.H. Prior, E. Rotenberg, J. Denlinger, T. Warwick, S.T. Manson, and H. Schmidt-Böcking, Phys. Rev. Lett. **76**, 2654 (1996).
[6] J.A.R. Samson, W.C. Stolte, Z.-X. He, J.N. Cutler, Y. Lu, and R.J. Bartlett, Phys. Rev. A **57**, 1906 (1998).
[7] L. Spielberger, O. Jagutzki, R. Dörner, J. Ullrich, U. Meyer, V. Mergel, M. Unverzagt, M. Damrau, T. Vogt, I. Ali, K. Khayyat, D. Bahr, H.G. Schmidt, R. Frahm, and H. Schmidt-Böcking, Phys. Rev. Lett. **74**, 4615 (1995).
[8] A.S. Kheifets and I. Bray, Phys. Rev. A **57**, 2590 (1998).
[9] A.Y. Istomin, N.L. Manakov, and A.F. Starace, J. Phys. B **35**, L543 (2002).
[10] J. Ahopelto, E. Rantavuori, and O. Keski-Rahkonen, Phys. Scr. **20**, 71 (1979).
[11] E.P. Kanter, R.W. Dunford, B. Krässig, and S.H. Southworth, Phys. Rev. Lett. **83**, 508 (1999).
[12] R. Diamant, S. Huotari, K. Hämäläinen, C.C. Kao, and M. Deutsch, Phys. Rev. A **62**, 052519 (2000).
[13] S.H. Southworth, E.P. Kanter, B. Krässig, L. Young, G.B. Armen, J.C. Levin, D.L. Ederer, and M.H. Chen, Phys. Rev. A **67**, 062712 (2003).
[14] M. Oura, H. Yamaoka, K. Kawatsura, K. Takahiro, N. Takeshima, Y. Zou, R. Hutton, S. Ito, Y. Awaya, M. Terasawa, T. Sekioka, and T. Mukoyama, J. Phys. B **35**, 3847 (2002).
[15] M. Ya. Amusia, E.G. Drukarev, V.G. Gorshkov, and M.P. Kazachkov, J. Phys. B **8**, 1248 (1975).
[16] R.C. Forrey, H.R. Sadeghpour, J.D. Baker, J.D. Morgan III, and A. Dalgarno, Phys. Rev. A **51**, 2112 (1995).
[17] E.G. Drukarev and M.B. Trzhaskovskaya, J. Phys. B **31**, 427 (1998).
[18] M.A. Kornberg and J.E. Miraglia, Phys. Rev. A **49**, 5120 (1994).
[19] A.S. Kheifets and I. Bray, Phys. Rev. A **58**, 4501 (1998).
[20] B. Krässig, M. Jung, D.S. Gemmell, E.P. Kanter, T. LeBrun, S.H. Southworth, and L. Young, Phys. Rev. Lett. **75**, 4736 (1995).
[21] M. Jung, B. Krässig, D.S. Gemmell, E.P. Kanter, T. LeBrun, S.H. Southworth, and L. Young, Phys. Rev. A **54**, 2127 (1996).
[22] O. Hemmers, G. Fisher, P. Glans, D.L. Hansen, H. Wang, S.B. Whitfield, R. Wehlitz, J.C. Levin, I.A. Sellin, R.C.C. Perera, E.W.B. Dias, H.S. Chakraborty, P.C. Deshmukh, S.T. Manson, and D.W. Lindle, J. Phys. B **30**, L727 (1997).
[23] N.L.S. Martin, D.B. Thompson, R.P. Bauman, C.D. Caldwell, M.O. Krause, S.P. Frigo, and M. Wilson, Phys. Rev. Lett. **81**, 1199 (1998).
[24] V.K. Dolmatov and S.T. Manson, Phys. Rev. Lett. **83**, 939 (1999).
[25] A. Derevianko, O. Hemmers, S. Oblad, P. Glans, H. Wang, S.B. Whitfield, R. Wehlitz, I.A. Sellin, W.R. Johnson, and D.W. Lindle, Phys. Rev. Lett. **84**, 2116 (2000).
[26] T. Khalil, B. Schmidtke, M. Drescher, N. Müller, and U. Heinzmann, Phys. Rev. Lett. **89**, 053001 (2002).
[27] B. Krässig, J.-C. Bilheux, R.W. Dunford, D.S. Gemmell, S. Hasegawa, E.P. Kanter, S.H. Southworth, L. Young, L.A. LaJohn, and R.H. Pratt, Phys. Rev. A **67**, 022707 (2003).
[28] E.P. Kanter, B. Krässig, S.H. Southworth, R. Guillemin, O. Hemmers, D.W. Lindle, R. Wehlitz, M.Ya. Amusia, L.V.

Chernysheva, and N.L.S. Martin, Phys. Rev. A **68**, 012714 (2003).
[29] O. Hemmers, R. Guillemin, E.P. Kanter, B. Krässig, D.W. Lindle, S.H. Southworth, R. Wehlitz, J. Baker, A. Hudson, M. Lotrakul, D. Rolles, W.C. Stolte, I.C. Tran, A. Wolska, S.W. Yu, M.Ya. Amusia, K.T. Cheng, L.V. Chernysheva, W.R. Johnson, and S.T. Manson, Phys. Rev. Lett. **91**, 053002 (2003).
[30] V.G. Gorshkov, A.I. Mikhailov, and V.S. Polikanov, Nucl. Phys. **55**, 273 (1964).
[31] A.I. Akhiezer and V.B. Berestetskii, *Quantum Electrodynamics* (Wiley, New York, 1974).
[32] E.J. Kelsey and J. Sucher, Phys. Rev. A **11**, 1829 (1975).
[33] V.G. Gorshkov, Zh. Éksp. Teor. Fiz. **47**, 352 (1964) [Sov. Phys. JETP **20**, 234 (1965)].
[34] V.G. Gorshkov and V.S. Polikanov, Pis'ma Zh. Éksp. Teor. Fiz. **9**, 464 (1969) [JETP Lett. **9**, 279 (1969)].
[35] M.A. Kornberg and J.E. Miraglia, Phys. Rev. A **48**, 3714 (1993).
[36] S.C. Mukherjee, K. Roy, and N.C. Sil, Phys. Rev. A **12**, 1719 (1975).
[37] H.A. Bethe and E.E. Salpeter, *Quantum Mechanics of One-and Two-Electron Atoms* (Plenum, New York, 1977).
[38] A. Bechler and R.H. Pratt, Phys. Rev. A **42**, 6400 (1990).
[39] J.W. Cooper, Phys. Rev. A **47**, 1841 (1993).
[40] L.D. Landau and E.M. Lifshitz, *Quantum Mechanics: Non-relativistic Theory* (Pergamon, Oxford, 1977).
[41] A.I. Mikhailov, I.A. Mikhailov, A.V. Nefiodov, G. Plunien, and G. Soff, Pis'ma Zh. Éksp. Teor. Fiz. **78**, 141 (2003) [JETP Lett. **78**, 110 (2003)].
[42] V.V. Anisovich, Usp. Fiz. Nauk **168**, 481 (1998) [Phys. Usp. **41**, 419 (1998)].
[43] A.I. Mikhailov, I.A. Mikhailov, A.N. Moskalev, A.V. Nefiodov, G. Plunien, and G. Soff, Phys. Lett. A **316**, 395 (2003).
[44] A.A. Radzig and B.M. Smirnov, *Reference Data on Atoms, Molecules and Ions* (Springer, Berlin, 1985).